Supplementary Materials for

Thermoelectric Properties of $YbZn_{(11-x)}Al_X$

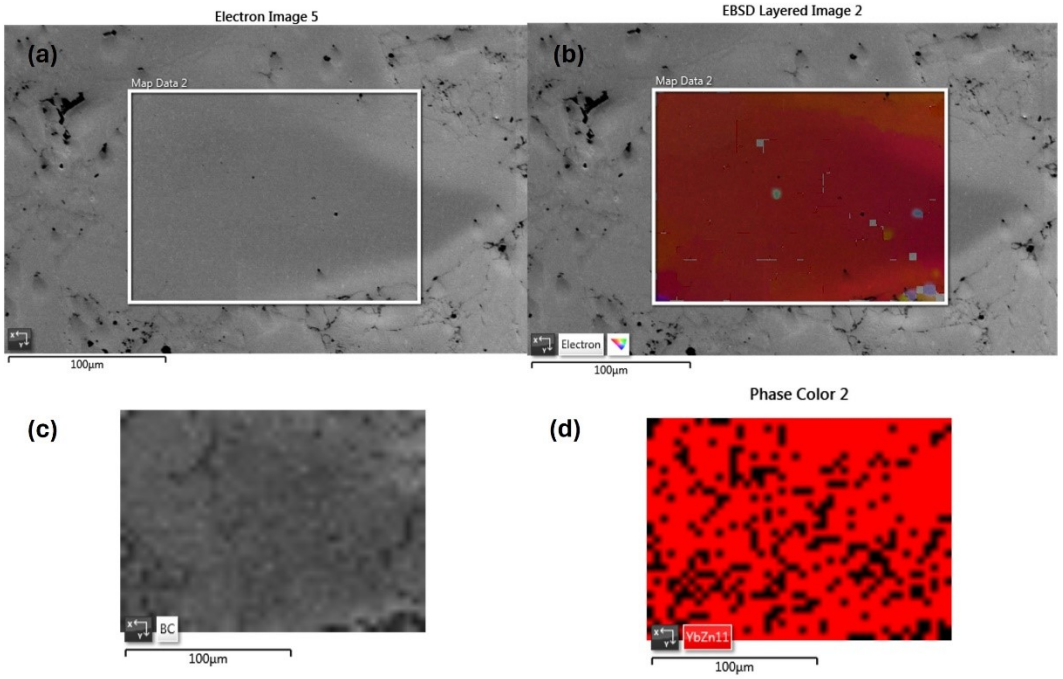

Figure S1: Electron Backscatter Diffraction(EBSD) results on $YbZn_{10.7}Al_{0.3}$, (a) electron image, (b) EBSD layered image, (c) Band structure image, (d) Phase color mapping. The red area indicates $YbZn_{11}$ diffraction (Kikuchi bands patterns) identified.

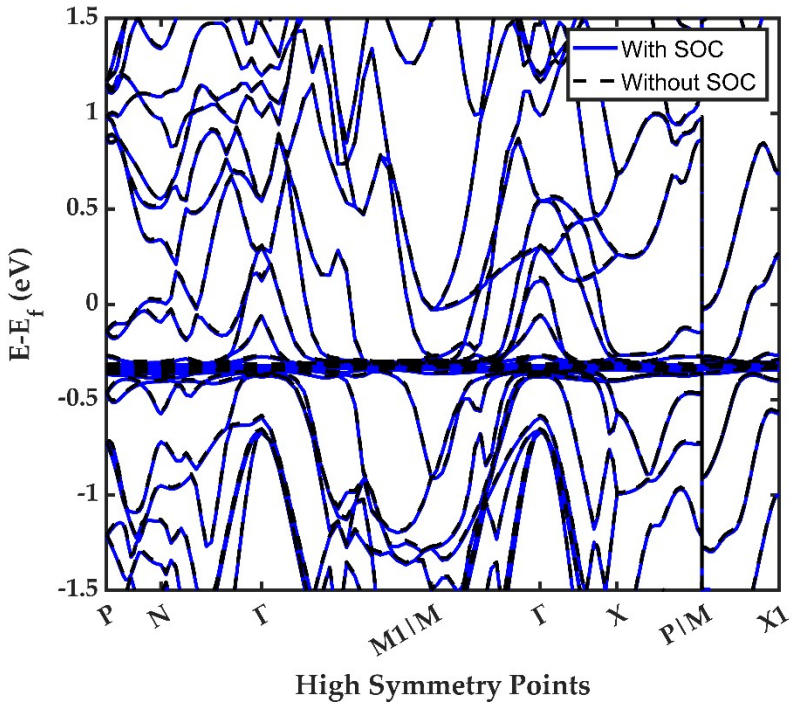

Figure S2: Band structure calculation with/without spin-orbit coupling (SOC) effects

Sample Stability and Uncertainty:

The $YbZn_{11}$ samples demonstrate reproducible results at low temperatures. However, upon annealing, exposure to high temperatures, and long exposure to ambient (air, moisture), the properties change. We also observe visible changes on the surface of the materials. While an in-depth analysis of sample stability is beyond the scope of this work, here we report the range of changes in the properties.

Figure S3 reports repeating the measurements for $YbZn_{10.7}Al_{0.3}$. First, we measured the sample as prepared in our lab and using Quantum Design Versalab as discussed in the main manuscript. This is reported as purple open circles. We then annealed the samples and remeasured the properties as shown in green squares. We noted a slight increase in the resistivity and the Seebeck coefficient and an improved power factor. We then shipped the samples to UH for high-temperature measurements, here represented by x. We note the resistivity is similar to our measured data, but the Seebeck coefficient is larger than what we measured. The data at UH was measured using ZEM3. Hence this can be partially related to instrument differences and partially due to sample exposure to ambient conditions for more than a month. Measurement dates are noted on the legend. Upon receiving the sample back, we polished the surface and remeasured the properties. Surprisingly, the results are very similar to our original measurements indicating the effect of annealing on Seebeck is eliminated, which could be attributed to the temperature history during the ZEM3 measurement. The ZEM3 measurement went up to 900K which is close to the annealing temperature, while the temperature changing rate could be distinguishably different, leading to the Al re-distribution and re-precipitation. Based on these 5 measurements performed on the same sample, we estimate uncertainty in Seebeck measurement to be 15% and 11% at 300K and 400K respectively where the maximum differences are observed. This estimation includes sample conditions and instrument errors and is consistent with ~10% error usually assumed for Seebeck measurements. The variations in the resistivity are smaller and are 8 and 9% respectively.

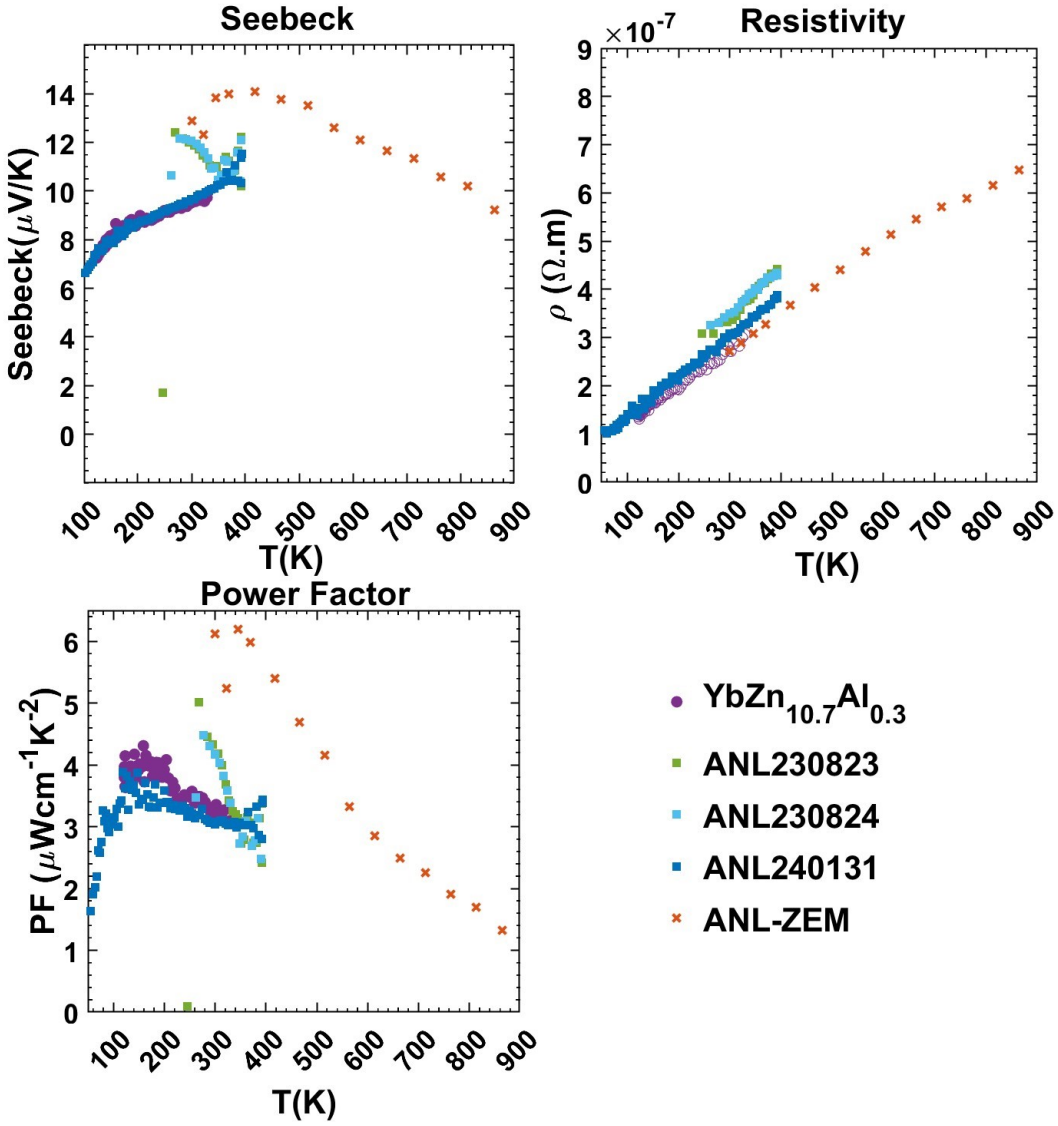

Figure S3: High-temperature (a) Seebeck, (b) resistivity, and (c) power factor of annealed/unannealed $YbZn_{10.7}Al_{0.3}$ samples. The ANL230823, ANL230824 samples are annealed samples measured on Quantum Design Versalab at the University of Virginia on August 23rd and 24th 2023. The ANL240131 sample is the same sample after the high-temperature measurement measured by Quantum Design Versalab at the University of Virginia on January 31st, 2024. The high-temperature measurement is done on ZEM3 by Xin Shi at the University of Houston.

Uncertainty in Seebeck calculations:

To address the uncertainties in our Seebeck coefficient calculations, we used the Mott formula based on the density of states (DOS), assuming a constant relaxation time. First-principles calculations inherently involve some uncertainty due to the usage of pseudopotentials, which are approximations for modeling the interactions between ions and core electrons. Various approximations, such as Local Density Approximation (LDA), Generalized Gradient Approximation (GGA), and Hybrid functionals (HSE, HSE06), with or without Spin-Orbit

Coupling (SOC) interactions (particularly relevant for heavy atoms), can lead to differences in the interaction between valence electrons and the core. These differences can alter the band structure and DOS near the Fermi level, thereby influencing the calculated Seebeck coefficient.[1]

As mentioned in the main text and illustrated in Figure S2, the inclusion of SOC does not significantly alter the band structure. However, a closer analysis of the DOS in Figure S4(a) reveals a subtle change in the slope near the Fermi level when SOC is considered, resulting in a difference of approximately ~6 μV/K in the Seebeck coefficient compared to calculations without SOC, as shown in Figure S4(b).

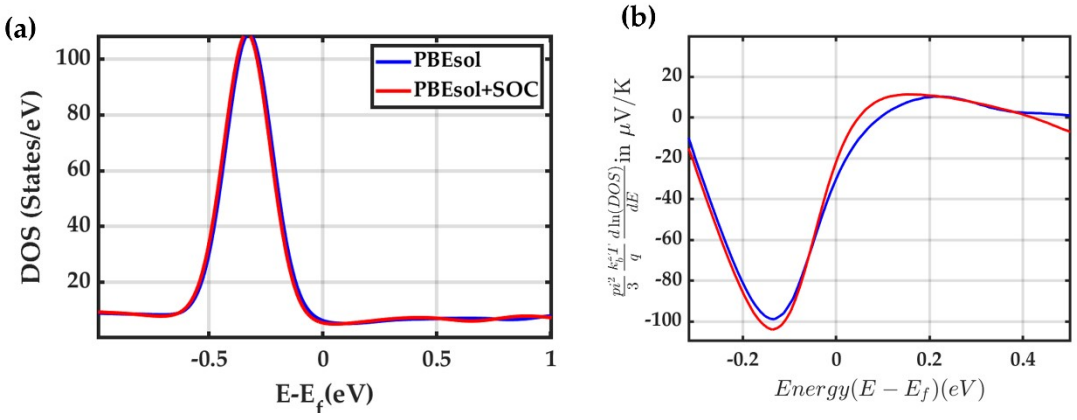

Figure S4: Spin-Orbit Coupling Effects on Seebeck.

In our calculation, we ensured consistency by using the same computational parameters for all defect calculations to minimize variability. For convenience, we excluded the effects of SOC in favor of faster calculations. As was discussed in the main text there are multiple other sources of error in Seebeck calculations, we discuss two main sources here:

1- Position of the Fermi level. Since the samples inherently contain defects, the position of the chemical potential is not priori known. In the case of $YbZn_{11}$, due to the fragile nature of the samples, thinning to perform Hall data to determine the position of the Fermi level experimentally was not possible. Below we show that by adding defects (Zn vacancy, or impurities) the chemical potential position can change resulting in different values of the Seebeck coefficient. As shown in Figure S5(a), in the presence of defects such as Zn vacancy and Al substituting Zn, the Seebeck coefficient can vary from the intrinsic value to larger (vacancy case) or lower (Al case). This shift impacts the Seebeck coefficient and is a crucial factor in interpreting experimental results. Simulating these effects precisely in first-principles calculations is challenging due to computational complexity and resource limitations as well as a lack of accurate information on the precise nature and concentration of the impurities in the experiment. Hence, theory can only provide general guidance and cannot predict the experimental values accurately.

2- Energy-dependent Relaxation times: The Mott Formula ($S = \frac{\pi^2}{3}\left(\frac{k_B^2 T}{e}\right)\left(\frac{1}{DOS}\frac{\partial DOS}{\partial \varepsilon} + \frac{1}{\tau}\frac{\partial \tau}{\partial \varepsilon}\right)_{\varepsilon=\mu}$) predicts the Seebeck coefficient to change not only with the DOS but also with energy-dependent relaxation times, $\tau(\varepsilon)$. Within constant relaxation time, the second term in the Mott

equation is neglected which can play a significant role when the Seebeck values are small. When ignoring the second term, and when chemical potential is fixed, the Mott equation predicts a linear increase in the Seebeck coefficient with respect to temperature (see Fig S6). While some of the samples show linear S with respect to T (e.g. $Yb_{10.6}Al_{0.4}Zn_{11}$), some others show a clear deviation from linear temperature dependence ($Yb_{10.8}Al_{0.2}Zn_{11}$) as shown in Figure 6 pointing to the significance of the second term.

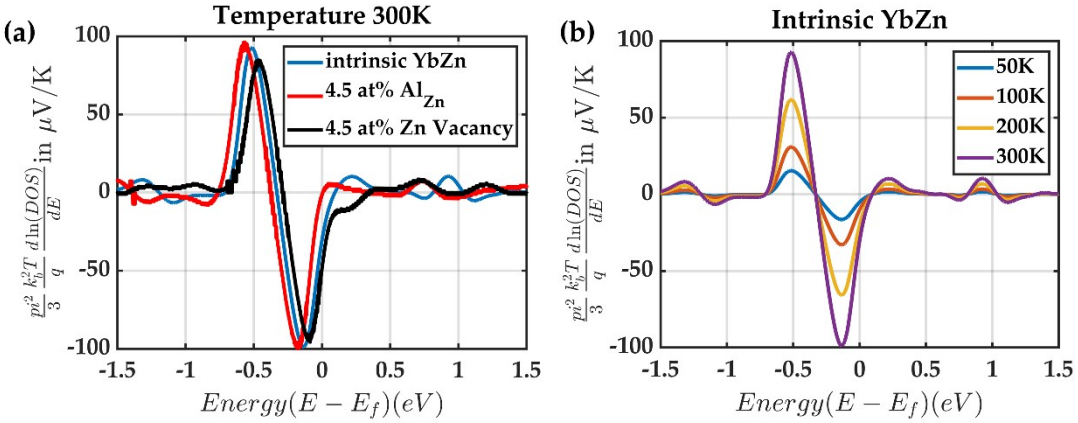

Figure S5: Sebeck coefficient with respect to defects and temperature.

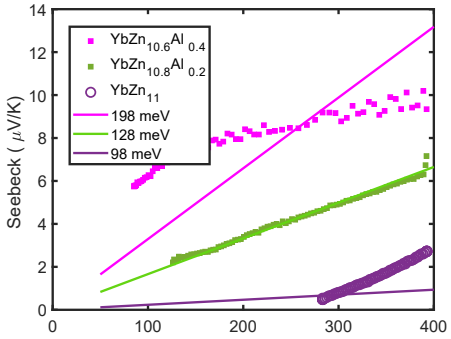

Figure S6. Seebeck coefficient vs temperature. Symbols are experimental data and lines are theoretical results obtained using the Mott Equation as applied to $YbZn_{11}$ and for different chemical potentials

ZT and effective thermal conductivity:

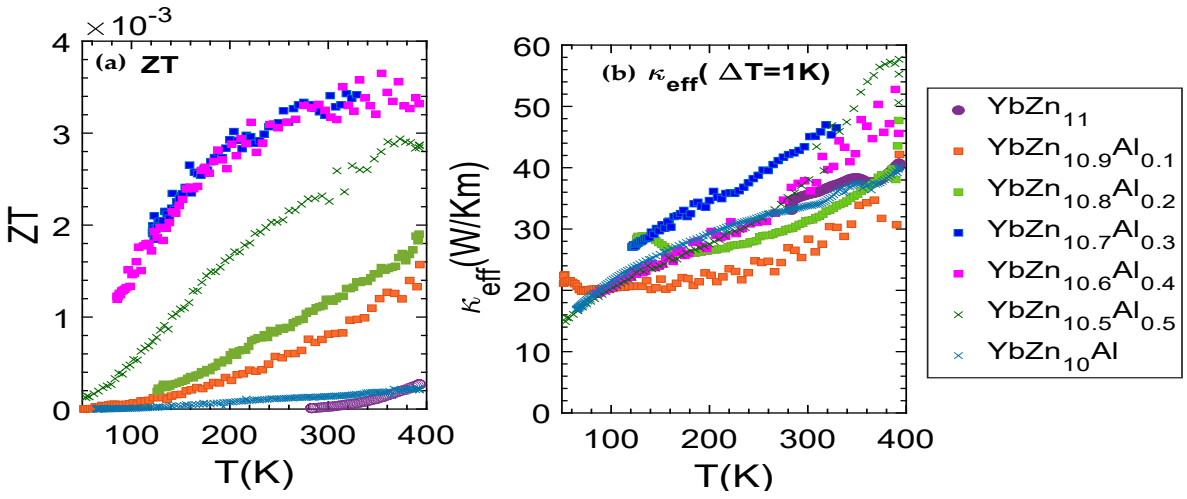

Figure S7: (a) figure of merit (ZT), (b) Effective thermal conductivity of $YbZn_{(11-x)}Al_x$ samples. ΔT is assumed to be 1K.

ZT values of $YbZn_{(11-x)}Al_x$ are low due to high thermal conductivity and relatively low power factor. The effective thermal conductivity $\kappa_{eff} = \left(\kappa + \frac{\sigma S^2 T_H^2}{2\Delta T}\right)$ at ΔT=1K can increase the passive thermal conductivity at 400K by a factor of 2.

Thermal conductivity analysis

Using the Wiedemann-Franz law to calculate the electronic thermal conductivity we observe that for most samples the electronic thermal conductivity is the dominant component. This is expected as the samples are metallic. However, $YbZn_{10}Al$ is an exception. The $YbZn_{10}Al$ sample contains Al above the solubility limit, leading to different reactions happening during the melting process, which results in the existence of oxide impurities such as SiO_2 (quartz crystal, from glass tube shards), ZnO (B3), and γ-Al_2O_3. The two latter oxides have higher electrical resistivity than $YbZn_{11}$ but also higher lattice thermal conductivity, ranging from 12W/m·K to 35W/m·K.[1,2]Therefore, the calculated lattice thermal conductivity of $YbZn_{10}Al$ sample doesn't fall in the similar range as lower Al concentration samples without oxide phases. Figure S9 shows the XRD of $YbZn_{(11-x)}Al_x$ samples and the oxide impurities in $YbZn_{10}Al$ can be identified.

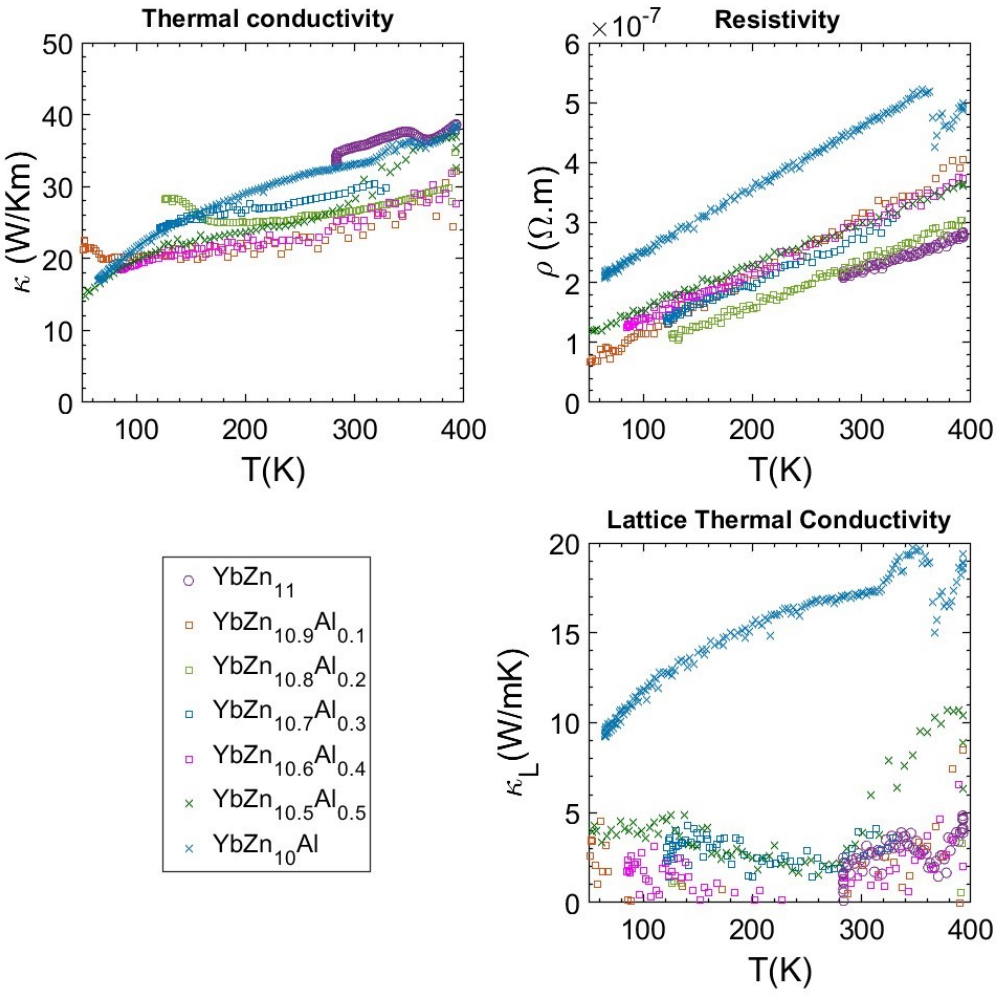

Figure S8: (a) Thermal conductivity, (b) resistivity, and (C) lattice thermal conductivity of $YbZn_{(11-x)}Al_x$ samples. lattice thermal conductivity calculated based on Wiedemann–Franz law using a Lorenz number of $L = 2.44 \times 10^{-8} V^2 K^{-2}$

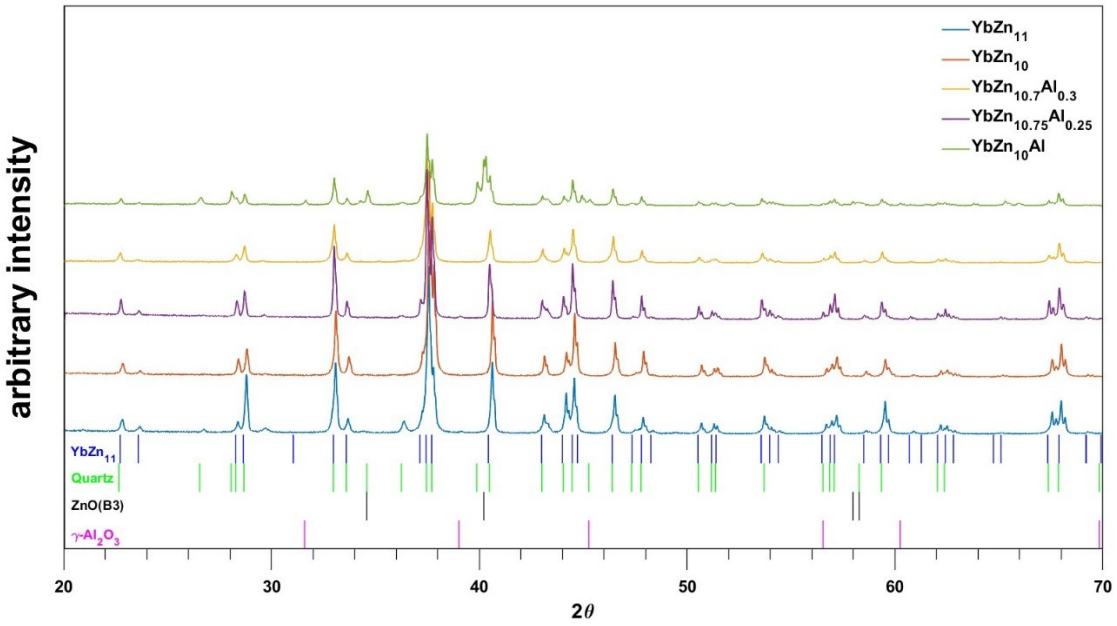

Figure S9 : XRD results for low-Al samples and $YbZn_{10}Al$, $YbZn_{10}Al$ contains peaks that can be identified as quartz(crystal), ZnO (B3), and γ-Al_2O_3. The abnormal resistivity and lattice thermal conductivity can be attributed to these oxide impurities.

Reference

1 Markov, M., Rezaei, S. E., Sadeghi, S. N., Esfarjani, K., & Zebarjadi, M. (2019). Thermoelectric properties of semimetals. Physical Review Materials, 3(9), 095401.

2 M. Vasheghani, E. Marzbanrad, C. Zamani, M. Aminy, B. Raissi, T. Ebadzadeh and H. Barzegar-Bafrooei, Heat and Mass Transfer/Waerme- und Stoffuebertragung, 2011, 47, 1401–1405.

3 CRC Handbook of Chemistry and Physics, Ed, William M. Haynes, 2016 , DOI:10.1201/9781315380476.